High-Z plasma facing components in fusion devices: Boundary conditions and operational experiences

R. Neu
Max Planck Institut für Plasmaphysik,
IPP-Euratom Association, Boltzmannstr.2, 85748 Garching, Germany

November 16, 2006

Abstract

In present day fusion devices optimization of the performance and experimental freedom motivates the use of low-Z plasma facing materials. However in a future fusion reactor, for economic reasons a sufficient lifetime of the first wall components is essential. Additionally, tritium retention has to be small to meet safety requirements. Tungsten appears to be the most realistic material choice for reactor plasma facing components (PFCs) because it exhibits the lowest erosion. But besides this there are a lot of criteria which has to be fulfilled simultaneously in a reactor. Results from present day devices and from laboratory experiments confirm the advantages of high-Z PFM but also point to operational restrictions, when using them as PFCs. They are associated with the central impurity concentration, which is determined by the sputtering yield, the penetration of the impurities and their transport within the confined plasma. The restrictions could exclude successful operation of a reactor, but concomitantly there exist remedies to ameliorate their impact. Obviously some price has to be paid in terms of reduced performance but lacking of materials or concepts which could substitute high-Z PFCs, emphasis has to be put on the development and optimization of reactor relevant scenarios which incorporate the experiences and measures.

PACS: 52.25.Vy, 52.40.Hf, 52.55.Rk, 52.55.Fa

1 Introduction

Large progress has been achieved in the performance and understanding of magnetically confined fusion plasmas and today fusion is at the gateway to prove its feasibility as a major energy source in the future. ITER [1], which will be launched most probably until the end of the year 2005, is designed to demonstrate the scientific and technical feasibility of magnetic fusion. Demo reactors (see for example [2]), which are being designed currently and which should be constructed in about 20 years from now, will incorporate all technical solutions necessary in a commercial reactor. By doing these steps, emphasis shifts from purely plasma oriented research to an integrated approach which has to aim not only at the optimization of the plasma performance but also at the adaptation to the technical boundary conditions.

Optimisation of the core plasma performance was the main driver for the implementation of low-Z carbon based materials as plasma facing materials (PFM) in almost all fusion devices during the last two decades. A large operational experience and database exists with these materials as plasma facing components, which allow a reliable prediction of the core plasma performance for future devices. However, as a part of the integrated approach, not only the contamination of the core plasma by impurities released from the walls must be kept below a critical level [3], but the plasma facing components (PFCs) have also to exhaust the α-particle fusion and external heating power together with the helium ash and to withstand off normal high heat loads from disruptions, vertical displacement events (VDEs), edge localised modes (ELMs) or runaway generation. For economic reasons a sufficient lifetime of the first wall components is essential. One of the most critical issues from the present view is the long term retention of the radioactive tritium fuel in the wall components which has to be limited and controlled for reasons of fuel supply, safety and also public acceptance of fusion energy [3]. The concerns and disadvantages of graphite materials are related to the latter points and, generally speaking, coupled with its chemical interaction with hydrogen and oxygen. Chemical erosion [4] leads to significant erosion yields even under low temperature, cold plasma conditions and can seriously limit the lifetime. A review on the current status of the use of carbon based PFC is found in [5]. Since the plasma is to a large extent a closed system, the released carbon impurities migrate long distances and can finally form thick deposits on special locations. These deposits are hydrogen rich and, as the tritium experiments in JET and TFTR have demonstrated, contain a major fraction of the total tritium fuel supplied to the machines [6, 7]. Extrapolation of the fuel retention to a steady state burning fusion plasma is difficult but we have to be prepared that retention

might be unacceptable and will not allow the operation of the device with tritium on a longer time scale [8, 9].
This is a very serious concern and calls urgently for reconsidering the choice of plasma facing components in general. The most promising alternative category of plasma facing materials are high-Z materials. These materials have acceptable thermo-mechanical properties, the possible advantage of very low or negligible erosion at low plasma temperatures and a moderate uptake of tritium [10]. These advantages compete with their strong poisoning effect of the plasma due to cooling by radiation losses, if the impurity source is too high and/or impurity transport leads to accumulation in the central plasma. After the first negative experiences due to strong central cooling through tungsten at the Princeton Large Torus (PLT) [11, 12] high-Z material was no longer used (except for high field/high density devices). Only recently, driven by the needs of a reactor, experiments using W as PFC were resumed. Although physics did not change over the years, alternative modes of operation, especially the use of a magnetic divertor and the application of special techniques to suppress excessive high-Z influx and accumulation, allowed to operate successfully with high-Z PFCs in several devices. Their results raise hope for the future use of high-Z PFM and further confirmation is expected from the planned 'ITER-like wall experiment' in JET, which will use Be, W and CFC in a configuration similar to that foreseen in ITER.
In the next section a brief overview on the general requirements, which have to be met by PFMs, will be given. Here, only tungsten will be treated in detail because at the moment only W is considered for further use in ITER or a reactor. After a short description of the early experiments, which led to the dropping of high-Z PFC, the paper will concentrate on the resent results from present day tokamaks. At the moment, only TEXTOR and ASDEX Upgrade perform experiments with W on a larger scale. Therefore, experiences with molybdenum from the high field tokamaks FTU and Alcator C-Mod will be presented as well. Although the detailled behaviour of Mo and W in plasma operation may differ, the general features are found to be similar. The final section will summarize the experiences and discuss the use of high-Z PFM and its consequences in future devices.

2 Boundary Conditions for W as Plasma Facing Material

The use of high-Z materials in general and particularly of tungsten as a PFM in a fusion device is primarily motivated by their thermo-mechanical properties and

density	19.3 g/cm^3
melting point	3410° C
vapour pressure (@m.p.)	$1.3 \cdot 10^{-7}$ Pa
therm. conductivity (@r.t.)	145 W/mK
electr. resistivity (@r.t.)	$5 \cdot 10^{-8}$ Ωm
DBTT	$100° - 400°$ C
thermal expansion	$4 \cdot 10^{-6}$/K

Table 1: Properties of tungsten.

their very low erosion under steady state operation conditions. However, besides these very specific advantages there are a lot of properties which are relevant in the fusion reactor environment. Each of them has to be addressed in specific experimental and theoretical approaches. Only a few of these properties can be covered here, as a complete assessment would go beyond the scope of this paper.

2.1 Material Properties

Critical issues are the mechanical properties of tungsten. Although its strength is high, its tensile elongation at room temperature is almost zero, making it brittle. The ductile to brittle transition temperature (DBTT) is far above room temperature, depending on the details of the manufacturing. In order to improve the brittleness several kinds of W based alloys have been developed. A concern for high heat flux components is the bonding between W armour and the heat sink. In the case of ITER copper alloys are proposed as the heat sink material. Copper exhibits a much larger thermal expansion ($16.5 \cdot 10^{-6}$/K) than W. In other to minimize stresses und resulting cracks castellated or 'brush'-like structures of W have been proposed.
In most present day devices inertial cooling is sufficient due to the short pulse durations. Also the particle fluencies and therefore the total amount of eroded material is low. This enables the use of W coatings on a graphite (or alternate) substrate. The coating techniques employed are chemical vapour deposition (CVD), physical vapour deposition (PVD), vacuum plasma spray (VPS) and inert gas plasma spray (IPS). These techniques result in different properties of the coatings. Whereas layers produced by CVD and PVD are homogeneous and dense as bulk tungsten, VPS and IPS coatings are porous and exhibit a reduced thermal conductivity [13].

In a reactor neutron irradiation will lead to activation and to changes in the mechanical properties of W [14, 15]. For the moderate neutron fluency of ITER (0.3-0.5 dpa, displacements per atom [14]) no critical deterioration of the performance of W as an armour material is foreseen. However, for the application of W in DEMO or a commercial reactor further R & D is required. The high energy of the DT-fusion neutrons opens up a broad class of nuclear reactions, as there are (n,γ), (n,p), (n,2n), (n,d) and (n,α). Since the integrated cross section of (n,γ) is higher than that of (n,2n), W will transmute to Re followed by Os. W becomes brittle after neutron irradiation due to radiation hardening and loss of strength at grain boundaries which lead to an increase in the ductile to brittle transition temperature (DBTT) [14]. Therefore, it is proposed to use W armour material without structural function and to optimise the geometry of the components to avoid crack initiation. Since significant generation of Re is expected, the thermal conductivity should be reduced during the lifetime of the component. Another critical issue is the decommissioning and waste. In general safety evaluations as [16, 17] the armour material is still kept open (Be or W). Although W has a much larger potential for the production of activation products, the two different choices do not show up strongly in the general accounting of the radioactive inventory due to the comparable small masses involved. Following [18] the radiotoxity contained in the ITER tungsten components requires that they have to be clearly treated as radioactive waste, but due to the rather small amount which is produced during the lifetime of ITER (95 tons) it is not considered a major drawback. Comparing the radiotoxity of the tungsten PFC's to values of the projected Be first wall, one finds that for the tungsten divertor plasma facing components it is already lower after 3 years and also decreases faster in time on a longer time scale.

2.2 Erosion Processes by Particle Loads

During steady state operation, erosion by particle fluxes is identified to be the main external impurity source. These eroding particles can be plasma and impurity ions from the edge plasma, as well as high energy particles from the core mainly as neutrals from charge exchange processes. For a given background plasma and location, the central impurity contamination depends linearly on the source. Therefore, low erosion rates not only lead to longer lifetimes of the PFCs, but also to a lower impurity content. Erosion due to particle bombardment depends on the mass ratio of incident particles to surface atoms, the particle energy and flux density, the surface temperature, and other factors, as for example the chemistry between the reaction partners.
Physical sputtering results from elastic energy transfer from incident particles to

target atoms. Surface atoms can be ejected, if enough energy is transferred to overcome the surface binding energy E_s. This energy originates directly from bombarding ions or through a collision cascade involving other target atoms. At low ion energies, where the transferred energy to surface atoms is comparable with the surface binding energy, the sputtering yield decreases strongly and becomes zero below a threshold energy. The theory of physical sputtering is well-understood [19] and the threshold energy, E_{th}, for the onset of sputtering from light projectiles on a substrate consisting of heavier species can be determined from momentum and energy conservation in an elastic collision:

$$E_{th} = \frac{(m_p + m_t)^4}{4 m_p m_t (m_p - m_t)^2} E_s \tag{1}$$

where m_p and m_t are the projectile mass and target mass respectively. For elements considered as plasma-facing materials the surface binding energy varies only by a factor of 2.5, while the atomic mass ranges from 9 AU (Be) to 184 AU (W). This makes the threshold energy for light ions strongly dependent on the target mass. For plasma-facing materials, such as C and W, experimental sputtering data exist for H, D and He in the energy range from 10 eV up to 10 keV and they are extended to higher energies and to tritium by computer simulations [20]. The energy distribution of sputtered atoms shows a mean value equivalent to $E_s/2$ [21] and therefore the energy of the sputtered atoms does not depend strongly on the material. Chemical reactions with incident hydrogen and oxygen ions can lead

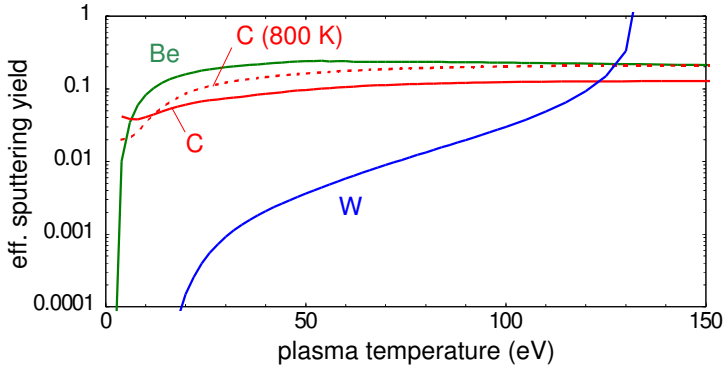

Figure 1: Erosion yield for Be, C, and W as a function of plasma temperature. Self-sputtering has been taken into account.

to the formation of volatile molecules. For carbon various chemical processes (see [22]) lead to a strongly enhanced erosion yield well below the threshold for physical sputtering (see Fig. 1). In principle, a chemically increased erosion yield could also be expected for tungsten by the formation of oxides with low surface binding energy. However, the amount of oxygen is greatly reduced in present day devices ($c_O \leq 1\%$) and the situation will improve even more in a fusion device with a higher duty cycle. Moreover, chemical erosion of W by O was found to be negligible in experiments [23] and in molecular dynamics calculations [24].
In a divertor device there is reduced plasma wall interaction in the main chamber and the plasma temperature in front of the divertor target plates can be de-coupled to some extend from the main plasma. In the foreseen 'semi-detached' operation in ITER, divertor plasma temperatures below 10 eV are envisaged. The sputtering thresholds for H, D and T on W are 447 eV, 209 eV and 136 eV, respectively, therefore the erosion by the background plasma during steady state phases will be negligible (see Fig. 1). However, as will be described below, it is not yet clear to what extent ELMs (edge localized modes) will appear. During these events the particle energy may be increased to values in the order of 1 keV. Another source of sputtering are impurities existent in the background plasma. These may be intrinsic impurities as W itself or light elements as C and O and seeded impurities (mostly noble gases) which are introduced to increase the edge plasma radiation and to cool the divertor plasma (see also Sec. 3). These impurities will have the ionic charge of A^{Z+} with $Z \approx 3-4$, because on their way towards the divertor they will not recombine completely. Therefore, they gain additional energy in the sheath potential in front of the targets and the thermal energy distribution will be shifted by $3ZkT_e$ (T_e: electron temperature). Consequently, the effective sputtering yield will be much higher as from the background plasma alone (see Fig.2). In the main chamber the ion flux to the walls is smaller but not negligible [25]. Additionally, hydrogen neutrals (CX) from charge exchange reactions will be present with energies far above the sputtering threshold [26].
The fluxes and energies of the particles expected in ITER [8,27] together with the consideration of off-normal events (see below), led to the present choice of PFMs in ITER, which foresees the use of Be in the main chamber, W at the divertor entrance and CFC at the divertor strike zones [1]. In a reactor, the most promising material solutions for the first wall armour seem to be tungsten as a coating on low activation steel, or low activation steel alone [28], since the erosion of Be, as planed in ITER, will be also too large.

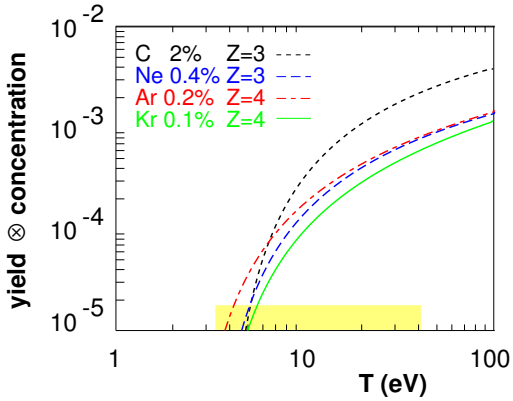

Figure 2: Tungsten sputtering yields for different species versus plasma temperature, assuming E_{impact} = 3ZT + 2T. Total yields are multiplied by the assumed concentrations to obtain realistic, effective yields per fuel ion flux. Charge states used for the calculation are given in the inset.

2.3 Arcs, Melt Losses and Dust

Electrical arcs are short duration ($<$ 1 ms) high current density ($\leq 10^{11}$ A/m^2) discharges that occur between the plasma and a PFC. The PFM is evaporated and eroded quickly with depths larger than 1 μm. To initiate an arc, the driving potential at the material surface must surpass the threshold $U_{arc} \approx 10-30$ eV, which is easily provided by the sheath potential of a 3-10 eV plasma [29]. These arcs are called 'unipolar' since they have only one solid electrode namely the wall acting as cathode. The other key element is an irregularity in the surface providing a hot spot, which is characterised by large local electric fields and reduced thermal conductivity leading to a faster heating up of the area and to thermal emission of electrons. The cathode spot is heated by ion impact and cooled by melting and evaporation, the source of the material erosion. The erosion rate of arcing is mainly given by the total current and most elements (including C and W) show a very similar ratio of eroded ion current to total arc currents which amounts to 10%. Typical dimensions of an arc are 10 μm in depth, 10-100 μm in width and 5-10 mm in length, resulting in 10^{17} - 10^{18} atoms of eroded material per arc event. Experimental results during the experiments with the W central column in ASDEX Upgrade show that about 5-10 % of the eroded material is due to arcing [30, 31]. Figure 3 shows a SEM picture of the surface of a 300 nm thick W coating after one experimental campaign.

The next step power producing device will be of the tokamak type and will have an elongated plasma shape. Therefore, there is the inherent possibility of disruptions in conjunction with a vertical displacement event (VDE). During this

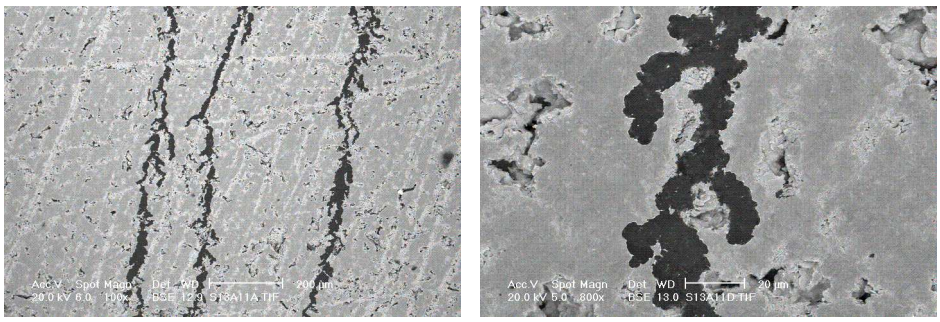

Figure 3: SEM picture (back scattered electrons) of the surface of a 300 μ nm W coated tile after one experimental campaign in ASDEX Upgrade.

process a major part of the stored energy will be deposited on the PFCs in about 1 ms leading to power densities in the order of 10 GWm^{-2}. Another reason for 'off normal events' with temporary high power loads are ELMs (edge localised modes), which are characteristic for the envisaged H-mode operation in a fusion reactor. Extrapolation from present day devices to ITER [32] show that a few percent of the core plasma thermal energy are deposited onto the divertor plate in a time of 0.1-1 ms leading to energy densities of about 1 MJm^{-2} and power densities above 1 GWm^{-2}, respectively [3]. Such large power densities can lead to melting and vaporisation of metallic surfaces. These melt layers are exposed to various forces such as electro-magnetism, surface tension, ablation recoil and so on [33]. The erosion rate during off normal events will be controlled and dominated by the evolution and hydrodynamics of these melt layers and vapour clouds. Although much modelling work has been done on this issue [34, 35], there is a lack of experimental confirmation since the present day devices do not have comparable power densities in off normal events. The simulation in other test devices is also difficult, due to the complex dynamics and its interplay with the strong magnetic field of a fusion device. The most relevant experiments are performed in plasma guns, which yield adequate energy densities [36]). The melt and vapour losses are calculated to be higher by far than the erosion by ordinary plasma impact in the divertor of a future burning plasma experiment as long as 'off normal events' cannot be excluded. However, following most recent experemental results and numerical simulations [37] even CFC (carbon-fibre compound) will be demaged macroscopically by the strongly different erosion of the matrix and the fibers. Therefore huge efforts are undertaken, to control and mitigate the effect of off-normal events.

As a result of the erosion processes mentioned above, dust will be produced. Al-

though dust has not been a concern in magnetic fusion devices, its amount will scale up by 2-3 orders of magnitude along with the erosion and the discharge duration. Therefore, it has to be accounted for in accident scenarios because chemical reactions of fine dust with steam and air create potential explosions and dispersal of radioactivity hazards [38]. In the case of carbon PFC the radiation hazard is caused by a large amount of co-deposited tritium, whereas the activated tungsten is a radiation safety issue in itself. Therefore, the maximum amount of W dust in ITER will be restricted to below 100 kg [39].

2.4 Displacement Damages, Hydrogen Retention and He-Bubble Formation

Charge exchange (CX) hydrogen neutrals with keV range energies can cause significant defects to accumulate in the tungsten lattice as demonstrated in experiments in the super conducting tokamak TRIAM-1M [40]. Dislocation loops, which form dislocation networks by interconnection have a negative impact on the structural integrity of the component. At the same time as interstitials, vacancies are formed by the knock-on damage, which can be saturated by implanted hydrogen. The micro-structural evolution of these dislocations/vacancies depends on irradiation temperature and material purity. According to recent laboratory experiments even hydrogen bubbles in W are formed during large fluency irradiation [41–43]. These bubbles may increase the hydrogen retention and give rise to an initial surface damage (blistering), which may then be increased by power load. The circumstances under which the growth of the bubbles is favoured, or how it may be hindered are not yet clear. Most recent investigations [44] lead to the conclusion that the observed blistering has to be attributed to the samples themselves, since it is only observed in cold rolled W foils, which are not relevant to reactor applications. The hydrogen retention in tungsten depends on several factors, such as material grade, fabrication process, temperature and ion energy (see for example [45]). The retained D is highest for temperatures at 400-500 K and decreases strongly with increasing temperature.
The helium produced in the DT-reaction is transported within the scarpe-off layer (SOL) from the bulk plasma towards the PFCs. Depending on the plasma temperature it leads to additional sputtering, or it can be implanted into the armour material. Recent investigations show bubbles and holes in W specimens irradiated by He ions with fluxes of about 10^{23} $m^{-2}s^{-1}$ (which are similar to those expected for ITER) and fluencies in the range of 10^{26} m^{-2} [46]. In contrast to this observation no blistering was observed in a similar experiment, but at lower sample

temperatures ($\approx$ 900 K instead of 1850-2850 K) [47]. Whether this different behaviour is due to the different temperatures leading to different He diffusivities and to a different vacancy concentration and mobility, or whether this is due to different W material grades has not been resolved yet. In contrast to low-Z PFMs the production of He by (n, α)-reactions within the bulk material will be of less concern in the case of W [48].

2.5 Impurities in the Plasma

In a zero dimensional model the condition for ignition is given as the balance of the power of the He nuclei produced in fusion reaction and the power losses through transport, which can be approximated by the empirical energy confinement time (τ_E) and the radiation losses (the plasma is optically thin for most of the frequencies). Additionally, the dilution of the fuel has to be considered when calculating the fusion power. Helium plays a distinct role in these considerations because power production and dilution are closely coupled via the residence time τ^*_{He} of the He ions in the plasma. This residence time is given by the transport of the He ash inside the plasma as well as by the probability by which the He is pumped once it reached the plasma edge. The area of the operational space critically depends on $\rho = \tau^*_{He}/\tau_E$. All light impurities are fully ionised in fusion relevant plasmas. Therefore the loss originating from impurity radiation is purely due to Bremsstrahlung (see high temperature part of radiation loss parameters in Fig. 4). However, in the case of the involvement of high-Z impurities, the radiation losses are dominated by line radiation, since high-Z elements will not be fully ionised. Therefore, the impurities have to be treated explicitely in the power balance investigations. Combining the equations for the production of fusion power and for the losses, one ends up with a cubic equation for the Helium concentration c_{He}, which is discussed to some extent in [51]. In general, two physically meaningful solutions exist for c_{He} at a given ρ. For $\rho \geq 15$ there is no stationary solution any more. ITER is designed to reach $\rho \approx 5$ [52], consistent with experiences from present day devices [53]. The operational space is also strongly limited by impurities originating from PFCs, which cause additional losses by radiation and dilution. Increasing their fraction, the operational window narrows quickly until there is finally no steady state solution at all. The maximum tolerable values are $\approx 3.0 \times 10^{-2}$ in the case of C and $\approx 2 \times 10^{-4}$ for W, however there is already a considerable reduction of the operational space for smaller concentrations [54, 55]. Fig. 5 shows the Z-dependence of the limit for the concentration which will prevent ignition, calculated under the assumptions as given above and

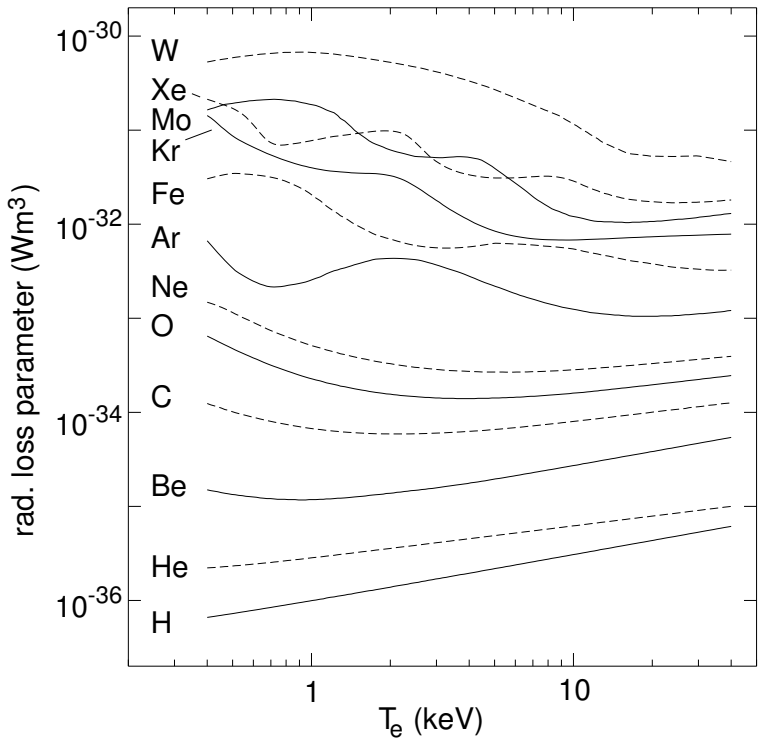

Figure 4: Radiation loss parameter calculated within the average ion model in coronal equilibrium [49, 50].

using the radiation loss parameters of [49, 50]. The fitted exponent should only serve as a guideline for the overall trend of the limit, since for high-Z elements, which are not fully ionised around the working point of the fusion reactor, the ionisation equilibria and the radiation will depend on the detailed structure of the ion. The value of the exponent $x = 2.2$ reflects the fact that the Bremsstrahlung, the recombination radiation and the losses by dilution are proportional to Z^2. It has to be pointed out that an ignited plasma has to be operated much below these limits in order to maintain a sufficiently large operational space. Most of the future devices foresee a material mix for the first wall components and the injection of low-Z or medium-Z elements to cool the plasma edge by radiation. This in turn will lead to even lower concentrations allowed for the individual impurities.

Seperate from the influx, the central impurity concentration depends strongly on transport, which is governed by the continuity equation (see for example [56]). Under steady state conditions in the source free region, which is easily fulfilled in the confined plasma under fusion relevant conditions, one gets for the impurity

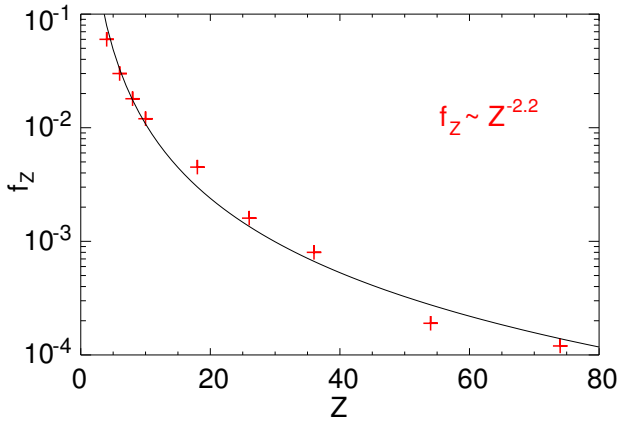

Figure 5: Z-dependence of the limit for the specific impurity concentration which will prevent ignition using $\rho = \tau^*_{He}/\tau_E = 5$ (see text).

density n_I^{eq}

$$\frac{1}{n_I^{eq}}\frac{dn_I^{eq}}{dr} = \frac{d\ln n_I^{eq}}{dr} = \frac{v}{D} \tag{2}$$

The diffusion coefficient D consists of an anomalous and a neo-classical part $D = D_{an} + D_{neo}$ and the convective contribution, which is a prerequisite for impurity accumulation and normally is assumed to be purely neo-classical with $v = v_{neo}$. Considering only collisions of impurity and main ions, one gets for the normalized impurity density gradient

$$\frac{d\ln n_I^{eq}}{dr} = \frac{d\ln n_D}{dr}\frac{Z_I}{Z_D}\frac{D_{neo}}{D_{neo}+D_{an}}\Big(1 - H\eta_D\Big), \tag{3}$$

where Z_I, Z_D are the charges of the impurity ions and the background ions and $H \approx 0.2 - 0.5$ represents the so called impurity screening, which depends on the collisional regime [57, 58]. $\eta_D = (\frac{d\ln n_D}{dr})/(\frac{d\ln T_D}{dr})$ is the ratio of the normalized temperature gradient and normalized density gradient of the background ions. From this equations one can easily see that, within the framework of this model, a necessary ingredient for impurity accumulation is a density gradient (density peaking) of the main ions. This gradient is amplified by $\frac{Z_I}{Z_D}$, which is typically 40-50 for W in plasmas of present day devices and will be ≈ 70 in a burning plasma. It is diminished through the anomal diffusion and the term in parenthesis. This term appears critical because it may vary from small positive numbers to small negative numbers: Typically the normalized temperature gradient is significantly larger than the density gradient in the confinement region and hence the product $H\eta_D$ is in the order of one. It is important to note, that within the neoclassical

theroy D_{neo} decreases with Z_I^{-2}. Therefore increasing D_{an} has a much stronger effect on the impurity density profile, than on the background plasma. Consecutively a small increase of D_{an} deteriorates the performance only weakly while suppressing strongly the high-Z contamination.

3 Operational Experiences in Earlier and Present Day Devices

Almost all fusion devices designed in the seventies started using the high-Z materials Mo or W for their limiters and other plasma facing components. By improving the vacuum and the conditioning of the vacuum vessel, which essentially means the reduction of oxygen and carbon and their compounds, the plasma properties improved, but at the same time strong central radiation from the high-Z material became evident. Eventually, this again led to a degradation and even to hollow electron temperature profiles. Following these observations the route for the PFCs diverged into two branches of tokamak devices: High field tokamaks ($B_t > 5-8$ T) operating at high current and high plasma densities kept the high Z-components. Tokamaks operating at moderate current densities, i.e. devices with larger cross sections exchanged their high-Z components for medium-Z materials (as stainless steel) and finally to low-Z materials as graphite or even beryllium. Previous reviews on the experiments and results with high-Z plasma facing components can be found in [5, 59, 60]. In the following results of the experiments which had the largest impact on the development from high-Z PFCs will be described in more detail (also see Table 2).

3.1 Early Devices with high-Z PFCs

The ORMAK tokamak (ORNL, Oak Ridge, 1973-1977; [67] and references therein) was operated with a W limiter and gold-plated liner. The emission of the W quasicontinuum from tokamak plasma was observed there for the first time [68]. Heating by NB counter injection always provoked major disruptions within 30-50 ms. The observed large radiation losses led to the test of low-Z PFCs in the successor experiments ISX-A and ISX-B [67].

The French tokamak TFR (CEA, Fontenay-aux-Roses, 1973 - 1986; [69] and references therein) went into operation in 1973 with a Mo ring limiter. The central energy losses were dominated by Mo radiation (typically $c_{Mo} \approx 10^{-3}$) and during NB (co-)injection the central radiation losses increased further. Similar to

Device	B_T T	I_P MA	R m	a m	τ_{pulse} s	P_{heat}^{aux} MW	High-Z PFC	Ref.
Earlier Devices								
Alcator C	12	0.8	0.64	0.17	0.5	1.5	Mo limiter	[61]
PLT	3.3	0.6	1.32	0.4	1	8	W limiter	[62]
Present Day Devices								
FTU	8	1.6	0.93	0.28	1.5	5	Mo, W test-limiter	[63]
Alcator C-Mod	8	1.5	0.67	0.22	1.5	6	all Mo PFCs	[64]
TEXTOR	2.6	0.5	1.75	0.46	10	8	Mo, W test-limiter	[65]
ASDEX Upgrade	3.2	1.4	1.65	0.50	10	28	W: 70% of PFCs	[66]

Table 2: Technical parameters of earlier and present day fusion devices.

other devices an anti-correlation effect between light and heavy impurities was found, apparently due to an increasing edge temperature for small low-Z impurity fractions. These experiences led to the installation of an inconel limiter, which decreased the central radiation losses considerably (typically $c_{Ni} \approx 10^{-3}$). However in ICR-heated plasmas it was observed that the confinement degraded again due to strong Ni influx and radiation. Finally this led to the installation of graphite limiters. The small tokamak DIVA (JAERI, Naka, 1974-1979; [70]) was the first experiment employing a poloidal magnetic divertor. It was initially equipped with an Au-plated limiter, an Au-plated liner and Cu/Mo divertor targets. Gold concentrations were estimated to amount up to $2 \cdot 10^{-3}$ [71]. A strong reduction of impurities and radiation was observed when operating with the divertor instead of limiters [72].

Alcator C (MIT, Cambridge, 1978-1983; [61]) was a high magnetic field limiter tokamak operated with Mo and graphite limiters and inconel walls. From bolometric measurements Mo concentrations of up to 1% were deduced in ohmic discharges with line averaged densities below 10^{20} m^{-3}. However, for higher densities (up to $5 \cdot 10^{20}$ m^{-3}) the concentration decreased by two orders of magnitude [61]. It was concluded [73] that physical sputtering by background ions as well as by Mo self-sputtering is the main source of Mo. Erosion by melting and subsequent evaporation could be excluded, since the power load and the Mo source-rate were strongly anti-correlated in the scans. Similar Mo influxes for D and He-plasmas, where CX-sputtering is less efficient, showed that erosion by energetic charge exchange particles did not play a strong role. ICRH experiments using stainless steel Faraday screens revealed a linear increase of the iron content

with ICRH power to values up to fractions of about $2 \cdot 10^{-3}$ [74]. As an explanation, sputtering from a thermal plasma was identified, the increased temperature of which was explained by an spurious absorption of ICRH power in the far edge plasma.

PLT (PPPL, Princeton) became operational in 1975 with tungsten limiters. After

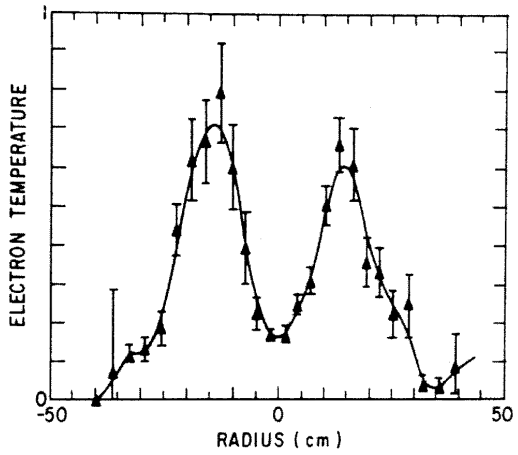

Figure 6: Hollow T_e profile measured due to excessive W radiation in a low density ohmic discharge in the PLT tokamak ($B_t = 3.2$ T, $I_p = 360$ kA, $n_e = 2.6 \cdot 10^{19}$ m^{-3}) [12].

removing light impurities as oxygen by special discharge cleaning, it soon became clear [11,12] that central tungsten radiation was occasionally as large as the ohmic input power and consequently led to hollow temperature profiles in hydrogen and deuterium discharges. In these cases, the W concentrations were estimated to be in the range of 10^{-3} [75]. The problem could only be solved by higher densities during plasma current ramp up to shrink the current channel, by edge cooling provided by impurities [62, 75] and to some extent also by titanium evaporation on the vessel walls (Ti-gettering) [76]. However, even in these cases a reduction by only about a factor of 5 of the W radiation was observed. The effect of the edge ion temperature was clearly demonstrated in [77], showing an increase of the W radiation by more than a factor of 5 when going from $T_i = 50$ eV to $T_i = 90$ eV. The observed increase of the W concentration with decreasing low-Z impurities points clearly to the fact that the edge operational space of PLT already led to a very strong erosion by background ions overriding the W sputtering from light impurities. In NBI-heated discharges the situation got even worse [77], so

that it was decided to exchange the W limiter for graphite and stainless steel limiters. Only a few discharges after the W limiters had been removed, the W level dropped below the detection limit [77], although a tungsten surface concentration of $\approx 15\%$ had been found by Auger analysis in deposited layers on the vacuum vessel surfaces [78]. This led to the conclusion that it was predominantly the direct plasma wall interaction at the limiter rather than the sputtering by charge exchange neutrals that led to the strong plasma contamination. Together with the results gathered in the ORMAK tokamak ([67] and references therein) these experiences finally led to the general use of low-Z plasma facing materials in devices operating at moderate field and current.

3.2 FTU

Initially, FTU was equipped with poloidal mushroom limiters made of Mo [79] which where exchanged to a full toroidal Mo limiter [80]. Mo concentrations of up to $c_{Mo} \approx 2 \cdot 10^{-3}$ at low plasma densities ($\bar{n_e} = 3 \cdot 10^{19}/\mathrm{m}^{-3}$) [81] and a decrease to $c_{Mo} \approx 2 \cdot 10^{-4}$ at ($\bar{n_e} = 7 \cdot 10^{19}/\mathrm{m}^{-3}$) [82] are reported. Surface conditioning by titanisation [82] and boronisation [81] leads to a strong (up to factor of 5) but transient reduction of the Mo concentration and Fe and Ni from vacuum chamber walls, are as abundant in the plasma as Mo [82]. Comparison of the plasma behaviour with different limiter materials or with a siliconised limiter [79] led to the conclusions, that the density limits and the onset of MARFE were strongly correlated with the presence of low-Z impurities and the very high density regimes could only be achieved with fully metallic plasma facing materials. The main production mechanism for metallic impurities was consistent with physical sputtering from background ions and self sputtering and the different sputtering yields are reflected in the specific impurity content in standard sawtoothing ohmic discharges, exhibiting very similar transport properties. The performance and main plasma parameters seemed not to be changed in the presence of the different limiter materials even when the radiation losses were centrally peaked, as in the case of W. High-Z accumulation was observed under ohmic conditions with the typical appearance of strong central radiation and hollow temperature profiles. In the start-up phase it can be avoided using a low ratio of I_P/n_e and by cooling the edge plasma during current ramp up by small amounts of Ne.

3.3 ALCATOR C-Mod

Alcator C-mod is equipped with a first wall and divertor tiles made entirely from molybdenum. For plasma densities below 10^{20} m^{-3} a rapid increase of the Z_{eff}

to values in the range of 3 was observed, partly attributed to a strong increase of the Mo concentration and the highest Mo levels are reached in low density limiter discharges. Comparison of ohmic discharges in FTU using Mo limiters with similar divertor discharges in Alcator C-Mod revealed that the Mo concentrations are lower by a factor of 2.5 [83], pointing to the beneficial properties of a divertor. In Alcator C-Mod the Mo concentrations are almost a factor of 10 lower during divertor operation than in limiter phases. The strong decrease of c_{Mo} with increasing density for L-Mode plasmas (limiter and divertor) is not so pronounced in H-Mode phases which suggest that besides the source, which generally decreases with increasing n_e due to lower edge temperatures, the transport in the plasma core becomes more important in H-Mode plasmas. A systematic study of c_{Mo} with P_{ICRH} and ICRH heating scenarios was performed in [83]. Under un-

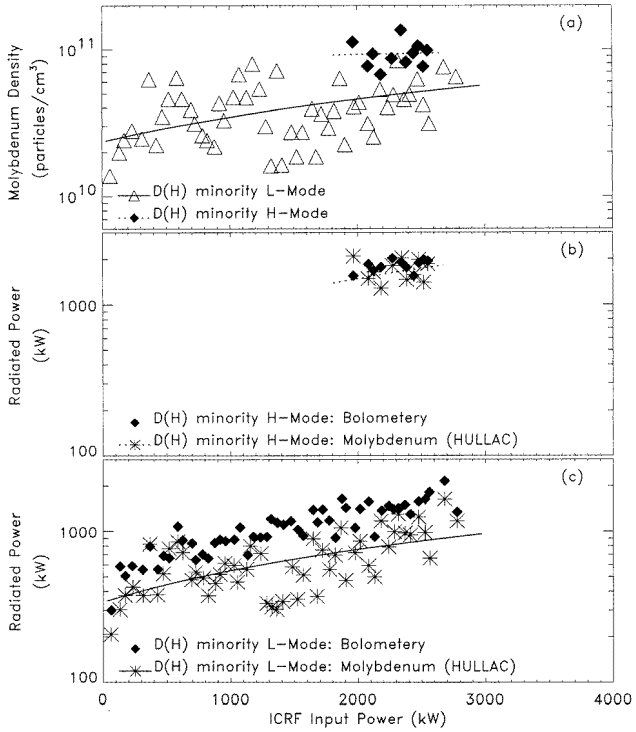

Figure 7: Molybdenum density against ICRF power during D(H) heated plasmas with H-mode and L-mode confinement in the Alcator C-Mod tokamak (a). Calculated radiated power (HULLAC) and measured total radiated power in H-mode (b) and L-mode plasmas (c) from (a) for $2 \cdot 10^{20} m^{-3} < n_{e0} < 3 \cdot 10^{20} m^{-3}$ [83].

boronised conditions a nearly linear increase of the Mo density and the radiated power with P_{ICRH} was observed. At a given ICRH-power the Mo density was

twice as high in H-Mode discharges compared to L-Mode discharges, reflecting the improved confinement (see Fig. 7). Additionally, it became evident that ICRH using monopole (single strap) antennae leads to a factor of ≈ 3 higher Mo content under otherwise similar conditions. For ohmic discharges a very good agreement between observed and simulated influx could by achieved when taking Mo self-sputtering and sputtering by $\approx$2% B^{3+} (from boronisation) into account [84]. However, in RF heated discharges the simulations underestimated the observed influx by up to a factor of three which was attributed to the production of a small fraction of energetic plasma ions or a non thermal electron distribution. An attempt has been made to gain a consistent picture of Mo influxes and resulting Mo content [85, 86]. It is concluded that the Mo source at the outer strike point zone dominates the Mo content during ohmic discharges and the influx from the inner wall, although large by number ($> 10^{18}$ s^{-1}) has only a small impact on the central. As dominant Mo sources for the central Mo concentration in ICRH heated plasmas the RF antenna screens were identified, which are close to the plasma and from which the Mo particles may have a high penetration probability. From the results of gas-puffing experiments [87] the authors conclude, that different drift patterns implying different friction forces and entrainment of the impurities and short connection lengths result in the different penetration.

3.4 TEXTOR

Tungsten and molybdenum were introduced into TEXTOR as a dome shaped test-limiter through a dedicated limiter lock [88, 89] or as a poloidal main limiter on a retractable mounting (10 W-coated tiles covering about 20% of the poloidal circumference) [90]. Most of the data were obtained with the test limiter 0.5 cm inside the radius defined by the main toroidal limiter and with 1.5 MW of neutral beam heating, resulting in power flux densities between about 8 and 12 MW m^{-2} [91]. The accumulation of high-Z impurities occurred very reproducibly under pure ohmic heating conditions [88] when a critical plasma density was reached (see Fig. 8), although the W and Mo limiters were loaded with only a fraction of about 4-6% of the total convective power. The behaviour was very similar for the Mo and W limiters and was characterised by rapidly growing radiation from the plasma centre, the development of flat or hollow temperature profiles and suppressed sawtooth activity. This led to internal disruption followed by a recovery period after which the accumulation could again occur [93]. The critical density for the onset of accumulation depended only weakly on the absolute amount of impurities released, which strongly suggests that the accumulation is driven by the internal impurity transport. In auxiliary heated plasmas ($P_{aux} > 1$MW) ac-

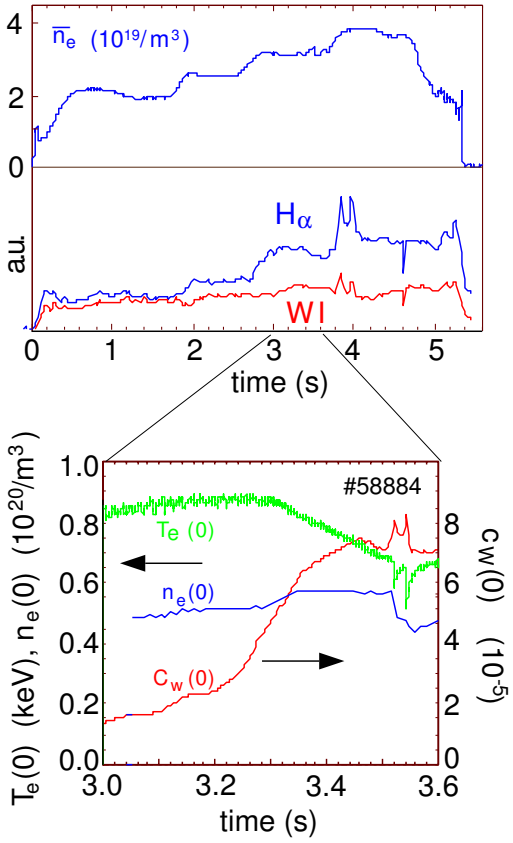

Figure 8: Evolution of W accumulation in ohmic plasmas in TEXTOR for critical plasma densities [92].

cumulation did not occur (with a few exceptions) neither when operating with Mo and W test limiters nor with the poloidal limiters with a plasma-sprayed W layer [90]. However, the W concentration in the core reaches values of several 10^{-4} at medium electron densities ($\bar{n}_e = 3-4\cdot 10^{19}$ m^{-3}) with a convective heat flux to the test limiter of typically $(2-5)\cdot 10^{-2}$ of the total heat flux. The observed local effective sputtering yield was about $2\cdot 10^{-2}$, indicating that a significant fraction of the released W entered the confined plasma. For a few cases with neutral beam injection (deuterium) W accumulation has been observed at low electron densities showing that the system can change into a state where accumulation can occur. The concentration of W or Mo in the core decreases strongly with increasing density, resulting in high-Z impurity concentrations below the detection limit ($< 10^{-5}$) at high densities. At intermediate densities, W accumulation occurs for such conditions at higher edge radiation levels ($> 65\%$), which was not observed

for Mo limiters under similar conditions. Central heating by ICRH was already seen to reduce central radiation and prevent high-Z accumulation when applied above a certain power threshold [94, 95]. The reduction of the edge temperatures in TEXTOR by neon seeding reduces the erosion yields, but the overall tungsten release does not decrease as additional sputtering of tungsten by neon occurs. A substantial decrease of the overall tungsten release occurs under radiation improved confinement conditions (RI-mode) due to reduced particle fluxes to the limiters and, as an additional effect, due to plasma edge cooling [96]. However, the reduction of the high-Z source strength under the RI-mode conditions is overcompensated by an increase of the high particle confinement times which led to increased high-Z impurity content.

3.5 ASDEX Upgrade

During the experimental campaign 1995/1996 a full toroidal tungsten divertor (VPS coated graphite, $d = 500\mu$m), was installed in ASDEX Upgrade and the discharges performed covered the full operational space of the ASDEX Upgrade tokamak [97]. The experiment demonstrated that the use of W-PFC in a fusion relevant divertor tokamak is feasible. The low sputtering yields for plasma temperatures below 20 eV and the high retention leads to low erosion and negligible migration of W into the main vessel [98]. A difference by a factor of 10 was found for the net and gross erosion under low temperature high density conditions [99, 100]. The much lower net erosion is attributed to 'prompt redeposition' as it was already observed in W marker experiments [101]: For high-Z materials the gyro-radius in the external field may be larger than the ionisation length, which can lead to deposition of the eroded particle directly after its erosion. The carbon concentrations were barely reduced due to the large carbon source from the inner graphite heat shield. Therefore, the erosion rates were strongly dominated by carbon, and strong C-deposition was found at the inner divertor target plates. Laboratory experiments and code simulations have shown [102, 103], that for carbon as a second impurity there is a delicate balance between enhanced W erosion and C deposition depending on the C concentration and the plasma temperature in front of the W PFC. In the vast majority of discharges ($c_W < 2 \cdot 10^{-5}$ in 80% of all H-Mode discharges) where no accumulation of tungsten was observed [104], the influence of the W divertor on the main plasma (density and the β limits, confinement, H-Mode threshold) was negligible [97]. The lowest W concentrations were found at high heating power and high plasma density and compatibility with radiating scenarios could be demonstrated. From the W behaviour in single discharges as well as from a statistical analysis of the W concentration of a large

ensemble of discharges [105], the impurity transport within the confined plasma was identified as the driving force behind the central c_W. The W divertor was removed in 1997 in the course of the installation of the closed divertor II. Since 1998 an increasing area of tungsten coated tiles ($d = 1 - 5\mu$m, plasma arc deposited) has been installed. Now the central column, the upper divertor, the lower divertor baffles and other PFCs at the low field side of ASDEX Upgrade, reaching an area of about 28 m^2 in 2004/2005 [54, 106, 107]. The behaviour of the light intrinsic impurities in ASDEX Upgrade has not yet changed significantly despite the exchange of 70% of the plasma facing components from graphite to tungsten, but a more pronounced dependence of the operation at low heating power on the conditioning is observed. This is expressed by a prolongation of ELM-free periods leading to increased central radiation and thereby to a feedback loop delaying the first ELM even further. Remedies to overcome this situation are to increase the heating power, or to enforce ELM activity by pellet injection [108]. Unlike in 'all-carbon' machines there is a huge difference in plasma radiation comparing limiter and divertor mode of operation, emphasising the crucial role of the divertor when operating with high-Z PFCs [109]. Although C influxes are found all over the central column [110], the limiter experiments as well as post mortem analyses of the tiles [31] prove that the W surface is not significantly covered. Against this background, the C-influxes seem to be in a highly dynamical equilibrium quickly building up during discharges. The tungsten concentrations range from below 10^{-6} up to 10^{-4}. The increased W-content during plasma current ramp-up rapidly decreases after X-point formation. In discharges with increased density peaking, increased central tungsten concentrations or even accumulation is observed. The region affected is very closely localized within $\rho_{pol} \leq 0.2$. Central heating leads to a strong reduction of the central impurity content [106, 111], which can be described quantitatively by neoclassical impurity transport simulations [112]. Simultaneously, only a very benign reduction of the energy confinement is observed (see Fig. 9).

4 Discussion and Conclusions

Currently, tungsten seems to be the most realistic material choice for reactor plasma facing components since it exhibits the lowest erosion rates while fulfilling other necessary engineering and safety criteria. Results from present day devices as well as from laboratory experiments point to the advantages of high-Z PFM but also to the price that has to be paid in the form of operational restrictions when using them for PFCs. The restrictions are associated with the parameters

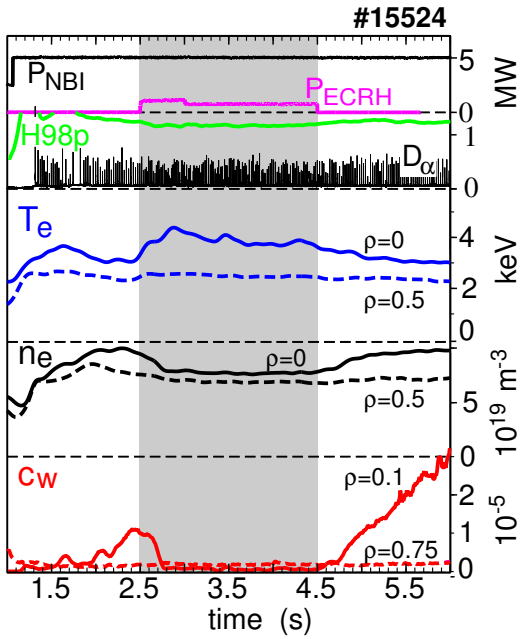

Figure 9: Behaviour of an improved H-Mode discharge in ASDEX Upgrade. The central W content could be suppressed by central ECRH, without strong influence on other plasma parameters.

which determine the central impurity concentration, namely the sputtering yield, the penetration of impurities and their transport within the confined plasma.
Hot edge conditions with a high low-Z impurity concentration lead to high sputtering yields and the corresponding low edge densities facilitate the penetration into the bulk plasma. Furthermore, a low ELM frequency supports the preferential penetration of impurities inside the edge transport barrier of H-modes. In the core plasma the combination of a peaked density profile and low anomalous diffusive transport causes central impurity accumulation.
Each of the above mentioned limitations could exclude successful operation of a reactor, but concomitantly there exist remedies to ameliorate their impact: In a reactor, high edge densities are a prerequisite for a technically feasible divertor operation. In turn this leads to low plasma temperatures in the divertor and consequently to low sputtering yields. In the main chamber, where the high SOL temperature will persist, the reactor may benefit from the broader SOL and its larger wall clearance compared to present day devices, which may reduce the penetration of impurities compared to that of the background plasma particles, which will propagate additionally by charge exchange. Large infrequent ELMs

will be forbidden in a reactor for target lifetime reasons. Here, active ELM pacemaking is required to reduce the ELM energy and avoid melting, but at the same time the edge transport will be increased periodically reducing impurity penetration. In the case of central density-peaking it is important to arrive at a condition where anomalous transport, which seems to be not or only weekly dependent on the charge of the ion, dominates over neoclassical transport [109]. Since neoclassical diffusion decreases with $1/Z^2$, this should not be a too serious condition in the case of W.

Although the operational restrictions imposed by the use of high-Z PFCs can be overcome by measures as described above, some price has to be paid in terms of reduced performance in most of the cases. However lacking of materials or concepts which could substitute high-Z PFCs, emphasis has to be put on the development and optimization of reactor relevant scenarios which incorporate the experiences and measures found in the present experiments.

References

[1] R. Aymar, P. Barabaschi, and Y. Shimomura, Plasma Phys. Controlled Fusion **44**, 519–565 (2002).

[2] R. Toschi, P. Barabaschi, D. Campbell, F. Elio, D. Maisonnier, et al., Fusion Eng. Des. **56-57**, 163 – 172 (2001).

[3] ITER physics basis editors, Nucl. Fusion **39**, 2137 – 2638 (1999).

[4] J. Roth, A. Kirschner, W. Bohmeyer, S. Brezinsek, A. Cambe, et al., J. Nucl. Mater. **337–339**, 970–974 (2005).

[5] V. Philipps, R. Neu, J. Rapp, U. Samm, M. Tokar, et al., Plasma Phys. Controlled Fusion **42**(12B), B293–B310 (2000).

[6] C. Skinner, E. Amarescu, G. Ascione, W. Blanchard, C. Barnes, et al., J. Nucl. Mat. **241-243**, 214–226 (1997).

[7] P. Andrew, D. Brennan, J. Coad, J. Ehrenberg, M. Gadeberg, et al., J. Nucl. Mater. **266-269**, 153 (1999).

[8] G. Federici, J. Brooks, D. Coster, G. Janeschitz, A. Kukuskhin, et al., J. Nucl. Mater. **290-293**, 260–265 (2001).

[9] G. Federici, P. Andrew, P. Barabaschi, J. Brooks, R. Dörner, et al., J. Nucl. Mater. **313–316**, 11–22 (2003).

[10] N. Yoshida, J. Nucl. Mater. **266 – 269**, 197 – 206 (1999).

[11] S. Suckewer and R. J. Hawryluk, Phys. Rev. Lett. **40**(25), 1649–1651 (1978).

[12] V. Arunasalam, C. Barnes, K. Bol, K. Brau, N. Bretz, et al., Recent Results from the PLT tokamak, in *Proc. 8th Conf. EPS, Prague 1977*, volume 2, pages 17–28, Geneva, 1978, EPS.

[13] S. Deschka, C. García-Rosales, W. Hohenauer, R. Duwe, E. Gauthier, et al., J. Nucl. Mater. **233–237**, 645–649 (1996).

[14] V. Barabash, G. Federici, M. Roedig, L. Snead, and C. Wu, J. Nucl. Mater. **283 –287**, 138 – 146 (2000).

[15] V. Barabash, G. Federici, J. Linke, and C. Wu, J. Nucl. Mater. **313-316**, 42–51 (2002).

[16] J. Raeder, I. Cook, F. Morgenstern, E. Salpietro, R. Bünde, et al., Safety and environmental assessment of fusion power (SEAFP), Technical Report EURFUBRU XII-217/95, European Commision, 1995.

[17] I. Cook, G. Marbach, L. Di Pace, C. Girard, and N. Taylor, Safety and environmental impact of fusion (SEIF), Technical Report EUR(01)CCE-FU/FTC8/5, European Fusion Develepment Agreement, April 2001.

[18] D. Cepraga, G. Cambi, M. Frisoni, and R. Forrest, Radiation transport and activation calculation in support for safety analyses of ITER-FEAT, Technical Report ERG-FUS/TN-SIC TR 07/2000, August 2000.

[19] W. Eckstein, C. García-Rosales, J. Roth, and J. Lázló, Nucl. Instr. Meth. **B83**, 95 (1993).

[20] W. Eckstein, C. García-Rosales, J. Roth, and W. Ottenberger, Sputtering Data, Rep. IPP 8/82, Max-Planck-Institut für Plasmaphysik, Garching, 1993.

[21] M. Thomson, Phil. Mag. **18**, 377 (1968).

[22] J. Roth, J. Nucl. Mater. **266-269**, 51 – 57 (1999).

[23] J. Roth, J. Bohdansky, and W. Ottenberger, Data on low energy light ion sputtering, Rep. IPP 9/26, Max-Planck-Institut für Plasmaphysik, Garching, 1979.

[24] I. Landman and H. Würz, J. Nucl. Mater. **313-316**, 77–81 (2003).

[25] A. Kallenbach et al., submitted to Plasma Phys. Control. Fusion (2005).

[26] H. Verbeek, J. Stober, D. P. Coster, and R. Schneider, Erosion of the Main Chamber Walls of Tokamaks by CX-Neutrals, in *Europhysics Conference Abstracts (Proc. of the 24th EPS Conference on Controlled Fusion and Plasma Physics, Berchtesgaden, 1997)*, edited by M. Schittenhelm, R. Bartiromo, and F. Wagner, volume 21A, part IV, pages 1457–1460, Petit-Lancy, 1997, EPS.

[27] G. Federici, R. Anderl, P. Andrew, J. Brooks, R. Causey, et al., J. Nucl. Mater. **266-269**, 14–29 (1999).

[28] H. Bolt, V. Barabash, G. Federici, J. Linke, J. Loarte, A. Roth, et al., J. Nucl. Mater. **307-311**, 43–52 (2002).

[29] H. Wolff, Arcing in magnetic fusion devices, in *Atomic and Plasma-Material Interaction Data for Fusion*, volume Vol. 1, Suppl. to Nucl. Fusion, page 91, Vienna, 1991, IAEA.

[30] W. Schneider et al., Tungsten Migration between Main Chamber and Divertor of ASDEX Upgrade, in *Europhysics Conference Abstracts (Proc. of the 28th EPS Conference on Controlled Fusion and Plasma Physics, Funchal, 2001)*, 2001.

[31] K. Krieger, A. Geier, X. Gong, H. Maier, R. Neu, et al., J. Nucl. Mater. **313–316**, 327–332 (2003).

[32] A. Loarte, G. Saibene, R. Sartori, D. Campbell, M. B*é*coulet, et al., Plasma Phys. Controlled Fusion **45**(9), 1549–1569 (2003).

[33] A. Hassanein, Fus. Technol. **15**, 513 (1989).

[34] A. Hassanein, G. Federici, I. Konkashbaev, A. Zhitlukhin, and V. Litunovsky, Fusion Eng. Des. **39-40**, 201 (1998).

[35] A. Hassanein and I. Konkashbaev, J. Nucl. Mater. **273**, 326 (1999).

[36] A. Makhanov, V. Barabash, and D. Mazul, I. Youchison, J. Nucl. Mater. **290-293**, 1117–1122 (2001).

[37] I. Landman, S. Pestchanyi, and B. Bazylev, Numerical Simulations for ITER Divertor Armour Erosion and SOL Contamination due to Disruptions and ELMs, in *Proc. of the 20th IAEA Conference Fusion Energy (CD-Rom), Vilamoura, Portugal, November 2004*, volume 0, pages IAEA–CN–116/IT/P23–6, Vienna, 2005, IAEA.

[38] D. Petti et al., J. Nucl. Mater. **233-237**, 37 (1996).

[39] G. Janeschitz, P. Barabaschi, G. Federici, K. Ioki, P. Ladd, et al., Nucl. Fusion **40**, 1197 – 1221 (2000).

[40] T. Hirai, K. Tokunaga, T. Fujiwara, N. Yoshida, S. Itoh, et al., J. Nucl. Mater. **258-263**, 1060 (1998).

[41] T. Venhaus, R. Causey, R. Doerner, and T. Abeln, J. Nucl. Mater. **290–293**, 505 (2001).

[42] W. Wang, J. Roth, S. Lindig, and C. Wu, J. Nucl. Mater. **299**, 124–131 (2001).

[43] M. Ye, H. Kanehara, S. Fukuta, N. Ohno, and S. Takamura, J. Nucl. Mater. **313-316**, 74–78 (2003).

[44] R. Causey, Hydrogen Retention and Release in Tungsten, Jülich, 2002, IAEA Technical Meeting on Atomic and Plasma-Material Interaction Data for Fusion Science and Technology.

[45] V. Alimov and B. Scherzer, J. Nucl. Mater. **240**, 75 (1996).

[46] D. Nishijima, M. Ye, N. Ohno, and S. Takamura, J. Nucl. Mater. **313 – 316**, 97 – 101 (2003).

[47] K. Tokunaga, R. Doerner, R. Seraydarian, N. Noda, Y. Kubota, et al., J. Nucl. Mater. **313 – 316**, 92 – 96 (2003).

[48] R. Behrisch, V. Khripunov, R. Santoro, and J. Yesil, J. Nucl. Mater. **258 - 263**, 686–693 (1998).

[49] D. Post, R. Jensen, C. Tarter, W. Grasberger, and W. Lokke, At. Data Nucl. Data Tables **20**, 397–439 (1977).

[50] D. Post, J. Abdallah, R. Clark, and N. Putvinskaya, Phys. Plasmas **2**, 2328 – 2336 (1995).

[51] D. Reiter, G. Wolf, and H. Kever, Nucl. Fusion **30**, 2141– 2155 (1990).

[52] D. Campbell, Phys. Plasm. **8**, 2041 – 2049 (2000).

[53] J. Hogan, J. Nucl. Mater. **241-243**, 68–81 (1997).

[54] R. Neu, R. Dux, A. Geier, O. Gruber, A. Kallenbach, et al., Fusion Eng. Design **65**(3), 367–374 (2003).

[55] R. Neu, Tungsten as plasma facing material in fusion devices, Technical Report 10/25, IPP, Garching, Germany, Dec. 2003.

[56] J. Wesson, *Tokamaks*, Clarendon Press, Oxford, 3 edition, 2003.

[57] S. P. Hirshman and D. J. Sigmar, Nucl. Fusion **21**(9), 1079–1201 (1981).

[58] R. Dux, Impurity Transport in Tokamak Plasmas, Rep. IPP 10/27, Max-Planck-Institut für Plasmaphysik, Garching, 2004.

[59] T. Tanabe, N. Noda, and H. Nakamura, J. Nucl. Mater. **196-198**, 11–27 (1992).

[60] N. Noda, V. Philipps, and R. Neu, J. Nucl. Mater. **241–243**, 227–243 (1997).

[61] B. Lipschultz et al., J. Nucl. Mater. **128-129**, 555 (1984).

[62] R. Hawryluk et al., Nucl. Fusion **19**, 1307 (1979).

[63] F. Alladio, B. Angelini, M. Apicella, G. Apruzzese, E. Barbato, et al., Overview of the FTU results, in *Proc. 18th IAEA Fusion Energy conference, Sorent*, volume IAEA-CN-77, page OV/2, Vienna, 2000, IAEA.

[64] M. Greenwald et al., Overview of the Alcator C-Mod Program, in *Proc. of the 20th IAEA Conference Fusion Energy (CD-Rom), Vilamoura, Portugal, November 2004*, volume 0, pages IAEA–CN–116/OV/2–5, Vienna, 2005, IAEA.

[65] U. Samm and the TEXTOR-94 Team, Plasma Phys. Controlled Fusion **41**, B57 – B76 (1999).

[66] A. Herrmann and O. Gruber, Fusion Science and Technology **44**(3), 569–577 (2003).

[67] ORMAK-ISX Group, Nucl. Fusion **25**, 1137 – 1143 (1985).

[68] R. Isler, R. Neidigh, and R. Cowan, Phys. Lett. **A63**, 295 (1977).

[69] TFR Group, Nucl. Fusion **25**, 1025 (1985).

[70] M. Tanaka, Nucl. Fusion **25**, 1073 (1985).

[71] S. Kasai, A. Funahashi, M. Nagami, and T. Sugie, Nucl. Fusion **19** (1979).

[72] S. Yamamoto, H. Maeda, Y. Shimomura, K. Odajima, M. Nagami, et al., Reduction of power loss due to heavy impurities in DIVA, in *Proc. 8th Conf. EPS, Prague 1977*, volume 1, page 33, Geneva, 1978, EPS.

[73] J. E. Rice, J. Terry, and E. Marmar, Nucl. Fusion **24** (1984).

[74] H. Manning, J. Terry, B. Lipschultz, B. LaBombard, B. Blackwell, et al., Nucl. Fusion **12**, 1665 – 1678 (1986).

[75] E. Hinnov, K. Bol, D. Dimock, R. Hawryluk, D. Johnson, et al., Nucl. Fusion **18**, 1305 (1978).

[76] H. Hsuan, V. Arunasalam, M. Bitter, K. Bol, D. Boyd, et al., Energy Balance of the PLT tokamak, in *Proc. 9th Conf. EPS, Grenoble 1978*, volume 2, pages 17–28, Geneva, 1978, EPS.

[77] K. Bol, V. Arunasalam, M. Bitter, D. Boyd, K. Brau, et al., Radiation, Impurity Effects, Instability Characteristics and Transport in Ohmically Heated Plasmas in the PLT tokamak, in *Proc. 7th IAEA Conf., Innsbruck 1978*, volume Vol.1, page 11, Vienna, 1979, IAEA.

[78] S. Cohen, H. Dylla, S. Rossnagel, S. Picraux, J. Borders, et al., J. Nucl. Mater. **76-77**, 459 (1978).

[79] M. Apicella, G. Apruzzese, M. Borra, G. Bracco, M. Ciotti, et al., Nucl. Fusion **37**, 381–396 (1997).

[80] M. Ciotti, C. Ferro, and G. Maddaluno, J. Nucl. Mater. **196 – 198**, 725 (1992).

[81] M. Apicella, G. Mazzitelli, G. Apruzzese, G. Bracco, B. Esposito, et al., J. Nucl. Mater. **313-316**, 269–273 (2003).

[82] M. Apicella, G. Apruzzese, R. De Angelis, G. Gatti, M. Leigheb, et al., Effects of wall titanium coating on FTU plasma operations, volume ECA Vol. 24B, pages 1573–1576, EPS, 2000.

[83] M. May, K. Fournier, J. Goetz, J. Terry, D. Pacella, et al., Plasma Phys. Controlled Fusion **41**, 45 – 63 (1999).

[84] D. Pappas, B. Lipschultz, B. LaBombard, M. May, and C. Pitcher, J. Nucl. Mater. **266-269**, 635 – 641 (1999).

[85] B. Lipschultz, D. Pappas, B. LaBombard, J. Rice, D. Smith, et al., Nucl. Fusion **41**, 585 – 596 (2001).

[86] B. Lipschultz, D. Pappas, B. LaBombard, J. Rice, D. Smith, et al., J. Nucl. Mater. **290-293**, 286 (2001).

[87] G. McCracken, R. Granetz, B. Lipschultz, B. LaBombard, F. Bombarda, et al., J. Nucl. Mater. **241 – 243**, 777 – 781 (1997).

[88] V. Philipps, T. Tanabe, Y. Ueda, A. Prospieszczyk, M. Tokar, et al., Nucl. Fusion **34**, 1417 – 1429 (1994).

[89] V. Philipps, A. Prospieszczyk, M. Tokar, B. Unterberg, L. Könen, et al., Experiments with molybdenum and tungsten limiters in TEXTOR, IAEA, Sevilla, 1994, IAEA-CN-60/A2/A4-P19.

[90] A. Pospieszczyk, T. Tanabe, V. Philipps, G. Sergienko, T. Ohgo, et al., J. Nucl. Mater. **290–293**, 947 – 952 (2001).

[91] A. Huber, V. Philipps, A. Pospieszczyk, A. Kirschner, M. Lehnen, et al., J. Nucl. Mater. **290 – 293**, 276 – 280 (2001).

[92] V. Philipps, M. Tokar, A. Prospieszczyk, U. Kögler, R. Koslowski, et al., Studies of high-Z wall components in TEXTOR94: local impurity release and its impact on the plasma core, in *Europhysics Conference Abstracts (Proc. of the 22th EPS Conference on Controlled Fusion and Plasma Physics, Bournemouth, 1995)*, volume 19C, part II, pages 321–324, Geneva, 1995, EPS.

[93] J. Rapp, M. Tokar, L. Könen, H. Koslowski, G. Bertschinger, et al., Plasma Phys. Controlled Fusion **39**, 1615–1634 (1997).

[94] G. Van Oost, A. Messiaen, V. Philipps, M. Wada, N. Hawks, et al., Influence of different heating schemes on high-Z contamination from a tungsten test limiter in TEXTOR, in *Europhysics Conference Abstracts (Proc. of the 21th EPS Conference on Controlled Fusion and Plasma Physics, Montpellier, 1994)*, volume 18B, part II, pages 1020–1023, Geneva, 1994, EPS.

[95] J. Rapp, G. Van Oost, G. Bertschinger, L. Könen, H. Koslowski, et al., Influence of high-Z limiter materials on the properties of the RI-mode in TEXTOR–94 with different heating schemes, in *Europhysics Conference Abstracts (Proc. of the 24th EPS Conference on Controlled Fusion and Plasma Physics, Berchtesgaden, 1997)*, volume 21A, pages 1745 — 1748, Geneva, 1997, EPS.

[96] B. Unterberg et al., J. Nucl. Mater. **266–269**, 75 (1999).

[97] R. Neu, K. Asmussen, K. Krieger, A. Thoma, H.-S. Bosch, et al., Plasma Phys. Controlled Fusion **38**, A165–A179 (1996).

[98] K. Krieger, H. Maier, R. Neu, and ASDEX Upgrade Team, J. Nucl. Mater. **266–269**, 207–216 (1999).

[99] K. Krieger, J. Roth, A. Annen, W. Jacob, C. S. Pitcher, et al., J. Nucl. Mater. **241–243**, 684–689 (1997).

[100] A. Thoma, K. Asmussen, R. Dux, K. Krieger, A. Herrmann, et al., Plasma Phys. Controlled Fusion **39**(9), 1487–1499 (1997).

[101] D. Naujoks, K. Asmussen, M. Bessenrodt-Weberpals, S. Deschka, R. Dux, et al., Nucl. Fusion **36**(6), 671–687 (1996).

[102] D. Naujoks and W. Eckstein, J. Nucl. Mater. **230**, 93 (1996).

[103] K. Schmid and J. Roth, J. Nucl. Mater. **313 - 316**, 302 – 310 (2003).

[104] K. Asmussen, R. Neu, R. Dux, W. Engelhardt, K. Fournier, et al., Investigations of Tungsten in the Central Plasma of ASDEX Upgrade, in *Europhysics Conference Abstracts (Proc. of the 24th EPS Conference on Controlled Fusion and Plasma Physics, Berchtesgaden, 1997)*, edited by M. Schittenhelm, R. Bartiromo, and F. Wagner, volume 21A, part IV, pages 1393–1396, Petit-Lancy, 1997, EPS.

[105] A. Geier, H. Maier, R. Neu, K. Krieger, and ASDEX Upgrade Team, Divertor Retention For Metallic Impurities at ASDEX Upgrade, in *Europhysics Conference Abstracts (CD-ROM, Proc. of the 28th EPS Conference on Controlled Fusion and Plasma Physics, Madeira 2001)*, edited by R. Pick, volume 25A, pages 169–172, Geneva, 2001, EPS.

[106] R. Neu, R. Dux, A. Geier, H. Greuner, K. Krieger, et al., J. Nucl. Mater. **313–316**, 116–126 (2003).

[107] R. Neu, R. Pugno, V. Rohde, R. Dux, T. Eich, et al., Assessment of Intrinsic Impurity Behaviour in ASDEX Upgrade, in *Europhysics Conference Abstracts (CD-ROM, Proc. of the 30th EPS Conference on Controlled Fusion and Plasma Physics, St. Petersburg, 2003)*, edited by R. Koch and S. Lebedev, volume 27A, pages P–1.123, Geneva, 2003, EPS.

[108] A. Kallenbach, P. T. Lang, R. Dux, C. Fuchs, A. Herrmann, et al., J. Nucl. Mater. **337-339**, 732–736 (2005).

[109] R. Neu, R. Dux, A. Kallenbach, T. Pütterich, M. Balden, et al., Nucl. Fusion **45**(3), 209–218 (2005).

[110] T. Pütterich, R. Dux, J. Gafert, A. Kallenbach, R. Neu, et al., Plasma Phys. Controlled Fusion **45**(10), 1873–1892 (2003).

[111] R. Neu, R. Dux, A. Geier, A. Kallenbach, R. Pugno, et al., Plasma Phys. Controlled Fusion **44**(6), 811–826 (2002).

[112] R. Dux, C. Giroud, R. Neu, A. G. Peeters, J. Stober, et al., J. Nucl. Mater. **313–316**, 1150–1155 (2003).